



## Original Article

## Autonomous exploration for radioactive sources localization based on radiation field reconstruction

Xulin Hu<sup>a</sup>, Junling Wang<sup>b</sup>, Jianwen Huo<sup>a,\*</sup>, Ying Zhou<sup>c,d</sup>, Yunlei Guo<sup>a</sup>, Li Hu<sup>a</sup><sup>a</sup> Robot Technology Used for Special Environment Key Laboratory of Sichuan Province, Southwest University of Science and Technology, Mianyang, 621010, China<sup>b</sup> School of National Defense Science, Southwest University of Science and Technology, Mianyang, 621010, China<sup>c</sup> Mianyang Central Hospital, NHC Key Laboratory of Nuclear Technology Medical Transformation, Mianyang, 621000, China<sup>d</sup> Department of Radiology, Mianyang Central Hospital, School of Medicine, University of Electronic Science and Technology of China, Mianyang, 621000, China

## ARTICLE INFO

## ABSTRACT

## Keywords:

Radioactive source localization  
Radiation field reconstruction  
Autonomous exploration  
Unmanned ground vehicles  
Gaussian process regression

In recent years, unmanned ground vehicles (UGVs) have been used to search for lost or stolen radioactive sources to avoid radiation exposure for operators. To achieve autonomous localization of radioactive sources, the UGVs must have the ability to automatically determine the next radiation measurement location instead of following a predefined path. Also, the radiation field of radioactive sources has to be reconstructed or inverted utilizing discrete measurements to obtain the radiation intensity distribution in the area of interest. In this study, we propose an effective source localization framework and method, in which UGVs are able to autonomously explore in the radiation area to determine the location of radioactive sources through an iterative process: path planning, radiation field reconstruction and estimation of source location. In the search process, the next radiation measurement point of the UGVs is fully predicted by the design path planning algorithm. After obtaining the measurement points and their radiation measurements, the radiation field of radioactive sources is reconstructed by the Gaussian process regression (GPR) model based on machine learning method. Based on the reconstructed radiation field, the locations of radioactive sources can be determined by the peak analysis method. The proposed method is verified through extensive simulation experiments, and the real source localization experiment on a Cs-137 point source shows that the proposed method can accurately locate the radioactive source with an error of approximately 0.30 m. The experimental results reveal the important practicality of our proposed method for source autonomous localization tasks.

## 1. Introduction

With the application and promotion of nuclear technology, radioactive sources are widely used in medicine, industry and other fields. As the high-energy rays emitted by radioactive sources may cause great harm to human body, the application of radioactive sources is strictly regulated by the laws of various countries and regions. However, during the period of 1993–2021, more than 3928 incidents of nuclear and other radioactive material out of regulatory control worldwide have been confirmed by the Illegal Traffic Database (ITDB) [1], such as the incident of accidental loss of radioactive source Ir-192 occurred in Nanjing [2]. In order to avoid social panic and casualties, it is necessary for technicians to search for uncontrolled radioactive sources as early as possible. Early source localization methods mainly relied on constructing a static or dynamic sensor network by deploying abundant sensor nodes in the

search area, and then the locations of radioactive sources are determined by the least square method [3,4] or the geometric method [5,6] based on extensive radiation observation data collected by the sensor nodes. For example, Huang et al. deployed multiple nuclear radiation detectors around a point source, and then used a linear-correction least-squares approach to achieve passive source localization in three-dimensional space [4]. Rao et al. proposed a geometric difference triangulation method to determine the location of the source based on the radiation measurements obtained by three sensors [6]. The maximum likelihood estimation method [7–9] is also used for the source parameter estimation, which can estimate the number and location of unknown radioactive sources utilizing a large amount of radiation data obtained from multiple sensors. In recent years, unmanned ground vehicles (UGVs) equipped with nuclear radiation sensors, such as Geiger-Müller counter and Sodium iodide detector, have been gradually

\* Corresponding author.

E-mail address: [huojianwen2008@hotmail.com](mailto:huojianwen2008@hotmail.com) (J. Huo).

adopted to search for radioactive sources due to their low risk and high flexibility. In order to improve the accuracy of source localization, suitable source localization methods are required to assist UGVs in determining the source locations.

Bayesian estimation method [10–15] is a commonly used source localization method. According to Bayesian criterion, the location of unknown radioactive source can be determined by solving the posterior probability distribution of source parameter vector which can be represented by the Markov chain Monte Carlo (MCMC) [10,11], particle filter [12,13] and other methods [14,15]. For example, Huo et al. introduced the MCMC method to approximate the posterior probability density function (PDF), and then designed an algorithm using the partially observable Markov decision process (POMDP) to automatically search for unknown radioactive sources through a mobile robot equipped with a Geiger-Miller counter and laser range sensor [10]. Ling et al. studied a strategy for distributed robots to collaboratively search for radioactive sources using a free energy strategy with adaptive step size, and proposed a particle filter algorithm based on particle fusion to estimate source parameters [13]. However, the Bayesian estimation method requires prior information of sources and a large amount of radiation observation data from sensors, which is not suitable for scenarios where there are multiple sources and can not effectively obtain the radiation intensity distribution of radioactive sources. In recent years, as an attractive research interest, locating unknown radioactive sources by reconstructing radiation field has aroused widespread attention in the field of radiation safety [16–20]. Abd Rahman et al. used a simple interpolation algorithm to reconstruct the radiation field of the region of interest and estimate the location of the unknown radioactive source by utilizing a robot armed with a Geiger–Müller (GM) counter [16]. Similarly, Royo and Li et al. used 2D interpolation algorithm for radiation mapping to locate uncontrolled radioactive sources with an unmanned aerial vehicle (UAV) carrying array detectors [17,18]. Liu et al. studied a fusion mapping algorithm that the reconstructed color-coded radiation map was projected onto the geometric environmental map to search for Alpha/Beta radiation sources in the environment [19]. Kishimoto et al. investigated a back-projection method to reconstruct the distribution of radioactive sources and locate unknown radiation source with sparse measurement data [20].

In order to improve the efficiency of source search, UGVs often have to possess the ability of efficient search, which means that suitable search strategies also are required to help UGVs better reconstruct the radiation field and then accurately locate unknown radioactive sources. The simplest search strategy was to scan the radiation area in a traversal manner to determine the source location. For example, in Ref. [17], an UAV moved in a traversal manner on the detection plane, and then the location of point radioactive source is estimated through the reconstructed radiation field. The advantage of this search strategy was that it did not require prior estimation of the source's parameters and the source localization accuracy was high, but the search efficiency was extremely low. In order to improve the search efficiency, the binary search method and the successive approximation search method were proposed in Ref. [18]. The binary search method was achieved by discarding half of the search area at a time, which significantly reduced the search time compared to the traversal search method. The time complexity of the successive approximation search method was lower than that of the binary search method, but it required a higher activity of the radioactive source, so that obvious changes in the dose rate could be detected at the boundary of the search area. Another search strategy was based on criteria to make an optimal decision in the current position of the UGV [21–23]. Li et al. designed a criteria that can make the robot move towards the rising direction of radiation gradient at each step until it converges to a static point which represents the source location [21]. Proctor et al. proposed a source search architecture based on the advantage actor critic (A2C) framework to automatically predict the next measurement point in the convex or non-convex environment [22]. Similarly, Liu et al. presented a convolutional neural network

architecture to make an optimal decision for the next measurement of the detector [23]. The third search strategy required the introduction of source parameter estimation methods. Then, combining the information gain methods [24–26], the UGV could make efficient decisions and finally reach the target position. For example, Ji et al. proposed a source search algorithm that particle filter is used to determine the source location, and A-star algorithm is used to predict the next measurement point [24]. Tomita et al. developed a path planning system that estimates the source parameters using the random forest algorithm to select the next measurement position of the robot by calculating the probability of eight directions [25]. Lin et al. adopted the artificial potential field method that the estimated source location as a target point generates the attractive force for mobile robots to determine the position of the next measurement point [26]. However, in real scenarios, if the source location estimated is not accurate, it is extremely difficult for UGVs to finally find the radioactive source.

Existing source localization methods have certain limitations and face several new challenges: (1) UGVs have to make appropriate path planning at the current state during the exploration process to improve the efficiency of source search, but most of the search strategies [16–18] are based on a predefined path, which cannot enable UGVs to perform autonomous source search; (2) technicians are eager to obtain the radiation field distribution in the environment to estimate the location of unknown radioactive sources. However, UGVs with limited perception capabilities can only perform limited radiometric measurements for a short exploration time. Therefore, it is challenging to find an effective reconstruction algorithm to reconstruct the radiation field with limited measurements and then precisely locate the radioactive sources; (3) existing source localization methods are inapplicable or have limitations for such scenarios where there is more than one source in the search area, such as two sources with same or different activity.

To overcome these challenges, this paper proposes an effective source localization method, abbreviated as PRE, to enable the UGV to autonomously explore for radioactive source localization in the environment through an iterative process: Path planning, Radiation field reconstruction and Estimation of source location. We adopt the Gaussian process regression (GPR) as the reconstruction algorithm to obtain the radiation distribution of radioactive sources, and design a reliable path planning algorithm to plan the exploration path of the UGV. The performance of the proposed method is further verified by theoretical analysis, simulation and real experiments. The main contributions of this paper are illustrated in the following points.

- (1) This paper proposes a source localization method which is suitable for UGVs that can only obtain sparse measurements within limited exploration time to solve the autonomous localization problem of radioactive sources.
- (2) A path planning algorithm which can enable UGVs to actively predict the next measurement point is designed to plan exploration paths and obtain effective radiation measurements. In addition, the reconstruction algorithm based on GPR is used to reconstruct the radiation field of radioactive sources, and the peak analysis method is introduced to estimate the number and location of radioactive sources.
- (3) In order to evaluate the localization performance of the proposed method, extensive simulation experiments are carried out. In addition, an UGV equipped with radiation detectors is used to carry out the real source localization experiment on the radioactive source Cs-137 with an activity of 1 mCi. Experimental results show that the source localization accuracy of the proposed method can reach approximately 0.3 m.

The remainder of this paper is organized as follows. In Section 2, we introduce the radioactive source localization task, the principle and mathematical derivation of path planning algorithm and radiation field reconstruction algorithm, and source location estimation method. In

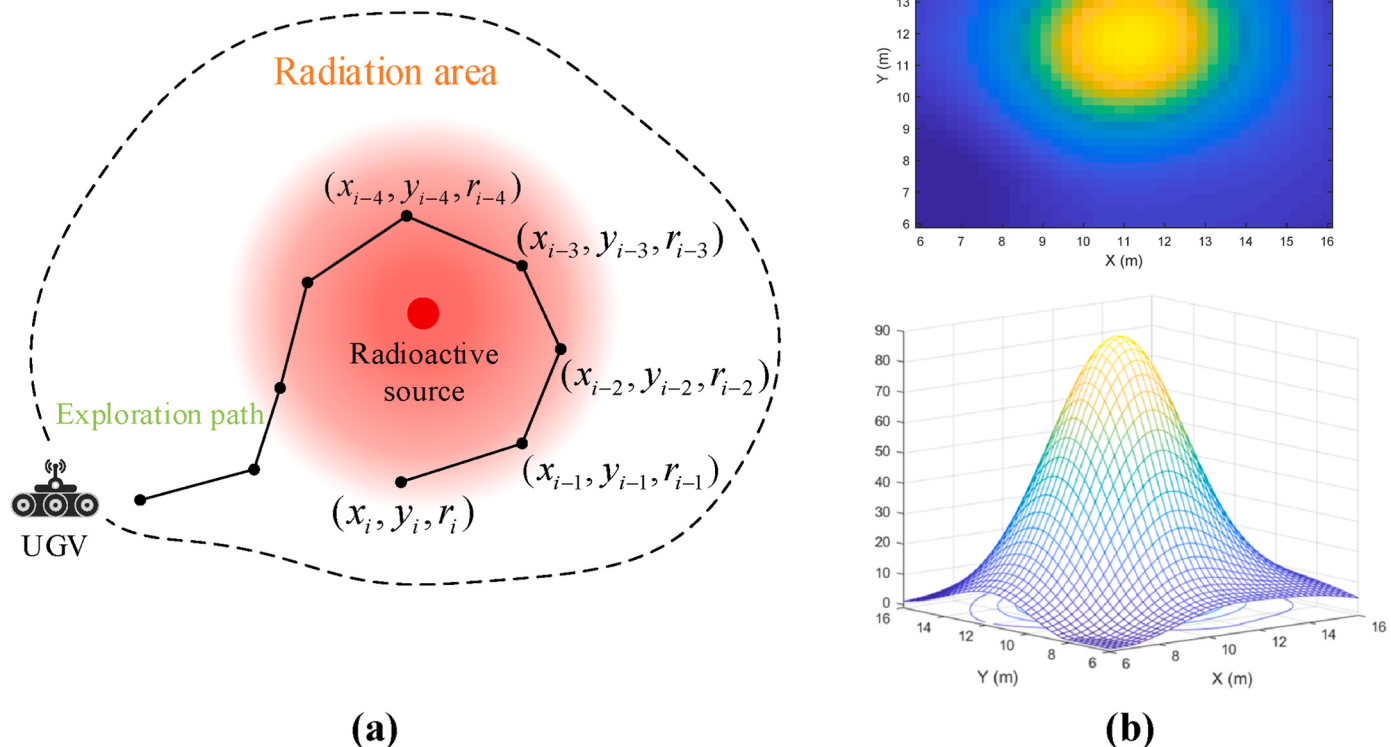


**Fig. 1.** Illustration of the source localization task. (a) Schematic diagram for locating the radioactive source with sparse measurements. The black dots indicate the radiation measurement points. (b) Approximate radiation field distribution of a single radioactive source in an occupancy grid map.

Section 3, the simulation and real experiment of locating unknown radioactive sources are carried out respectively, and the localization accuracy of the proposed method in the scenarios of one and two radioactive sources are respectively analyzed. In Section 4, the conclusions are made and possible future steps are discussed.

## 2. Materials and methods

### 2.1. Source localization task

While entering the radiation area, the UGV requires to autonomously plan the exploration path and perform radiation measurements. The radiation signal emitted by radioactive source can be detected by the radiation sensor equipped on the UGV. However, due to the limited exploration period and limited sensing abilities of the radiation sensor, the UGV is only able to obtain sparse radiation measurements. In order to accurately locate the radioactive source, the UGV needs not only effective radiation field reconstruction algorithm to reconstruct the radiation field, but also appropriate path planning algorithm to automatically predict the next measurement point. The schematic diagram for locating the radioactive source with sparse measurements is shown in Fig. 1(a). Let the three-value vector  $(x_k, y_k, r_k)$  represents the coordinate  $(x_k, y_k)$  and the radiation measurement value  $r_k$  of the  $k$ -th measurement point ( $1 \leq k \leq i$ ,  $k \in \mathbb{Z}$ ). The measurement data and their corresponding coordinates are used to reconstruct the radiation field distribution around the radioactive source. Then, the source parameters (i.e., number of sources and their respective locations) of radioactive sources are estimated based on the reconstructed results.

In order to approximate the radiation field distribution of radioactive sources in real environment, the physical process of ray transport in matter is simulated by Geant4 program based on Monte Carlo (MC)

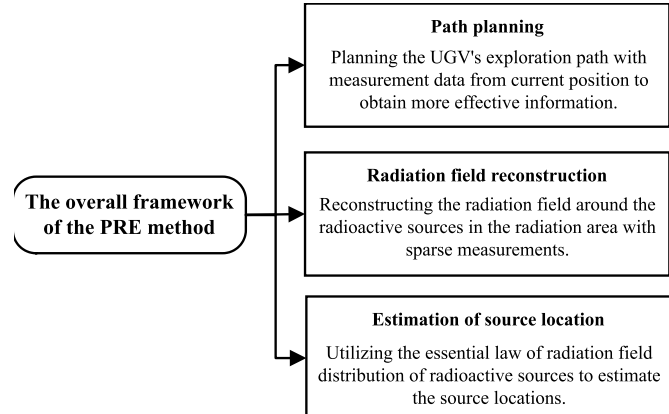


**Fig. 2.** The overall framework of the PRE method.

method. Geant4 program is widely used in nuclear technology, space physics, nuclear physics and other fields [27]. In the simulation environment, the detector model is not considered. Since the UGV's detection position is usually at a certain height from the ground, it is necessary to count the radiation field (or energy deposition) distribution of gamma rays in the detection plane through Geant4 simulation. In addition, the detection plane is represented as an occupancy grid map, and the center of the grid denotes the radiation measurement point, as shown in Fig. 1(b).

### 2.2. The PRE method

Existing methods usually require remote control of UGV to collect

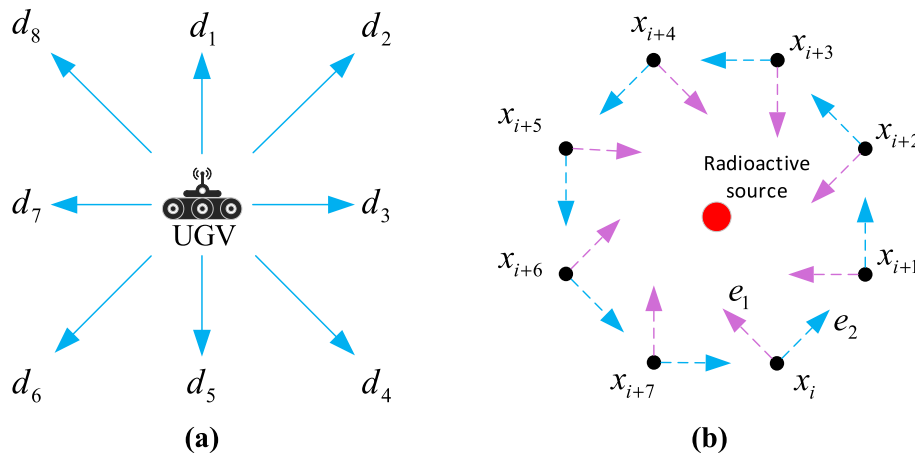


**Fig. 3.** (a) Selection of movement direction of the UGV in the occupied grid map. (b) Schematic diagram of the UGV moving around the radioactive source and measuring radiation data. The black dots indicate the radiation measuring positions; the magenta arrows represent the vector  $e_1$ ; the blue arrows represent the vector  $e_2$ . The execution of the path planning algorithm is terminated when the exploration path forms a closed loop. (For interpretation of the references to color in this figure legend, the reader is referred to the Web version of this article.)

extensive radiation data to draw radiation map and then locate radioactive sources [17,18]. To overcome this challenge, this paper proposes the PRE method to enable the UGV to explore autonomously in the radiation area, then reconstruct the radiation field and finally determine the source locations. The overall framework of the PRE method is shown in Fig. 2. First, in order to obtain more effective radiation information, a path planning algorithm is required to plan the UGV's exploration path in the radiation area with measurement data from the current position (or including previous positions). Then, based on acquired measurement data and their corresponding positions, a radiation field reconstruction algorithm is applied to reconstruct the radiation field around the radioactive sources. Further, based on the reconstructed result, the respective locations of the sources are estimated according to the basic principles of radiation field distribution of radioactive sources. The details of the PRE method are presented in the remainder of Section 2.2.

#### 2.2.1. The designed path planning algorithm

In order to achieve autonomous localization of radioactive sources, the UGV must have the ability to automatically predict the next measurement position. In addition, in order to effectively reconstruct the radiation field around radioactive sources and achieve accurate localization of the sources, the UGV initially is required to approach the radioactive sources to obtain sufficient number of incident events or energy deposition through the radiation sensor, and then moves along a path around the sources. Therefore, an appropriate path planning algorithm is designed to meet the above requirements.

The path planning algorithm is mainly composed of two levels. The first level is that the UGV gradually approach the sources utilizing the gradient ascending search strategy which can guide the UGV to move in the direction where the radiation gradient rises fastest. The radiation gradient is defined as  $\frac{dr}{dl}$ . Among them,  $dl$  represents the distance between the measurement position and the current position, and  $dr$  represents the radiation values measured within the time interval  $\Delta t$ . Since the UGV can move in eight directions:  $\{\uparrow, \nearrow, \rightarrow, \searrow, \downarrow, \swarrow, \leftarrow, \nwarrow\}$  in the occupied grid map (Fig. 3(a)), the radiation gradients in the eight-neighbor directions can be expressed as  $(g_1, g_2, g_3, g_4, g_5, g_6, g_7, g_8)$ . To avoid the UGV falling into a local optimum, an adjustment factor  $q$  is introduced to control the randomness of the decision process, and then the radiation gradients are converted into the probability of moving in each direction:

$$(d_1, d_2, d_3, d_4, d_5, d_6, d_7, d_8) = \text{softmax}\left(\frac{g_1, g_2, g_3, g_4, g_5, g_6, g_7, g_8}{q}\right) \quad (1)$$

where  $\text{softmax}(\cdot)$  represents the normalized exponential function. When

the radiation measurement at the current position exceeds the set threshold  $E$ , the second level of the path planning algorithm will be executed to enable the UGV to plan the exploration path around radioactive sources. Similarly, the UGV will calculate the radiation gradient of eight-neighbor directions and determine which direction the gradient rises fastest. Then, the vector in the fastest direction of gradient rise is set to  $e_1$ . Set the center coordinates of the eight grids around the  $i$  th measuring point ( $x_i$ ) as  $z_k$  ( $1 \leq k \leq 8, k \in \mathbb{Z}$ ). Thus,  $e_1$  can be calculated by

$$e_1 = z_{\text{argmax}(g_k)} - x_i \quad (2)$$

where  $\text{argmax}(g_k)$  represents the variable  $k$  corresponding to the maximum value of  $g_k$  ( $1 \leq k \leq 8, k \in \mathbb{Z}$ ). In particular, it is specified that  $e_2$  is in the clockwise direction of  $e_1$  and orthogonal to  $e_1$ , and the modules of the vectors  $e_2$  and  $e_1$  are equal, that is, if the vector  $e_1$  is  $(m, n)$ , the vector  $e_2$  can be expressed as  $(n, -m)$ , as shown in Fig. 3(b).

Initially, the UGV will move towards the direction of the vector  $e_1$  to approach the radioactive source. When the measured radiation value exceeds the threshold  $E$ , the second level of the path planning algorithm is executed. At this time, the direction of movement of the UGV will change from the vector  $e_1$  to the vector  $e_2$ . After that, if the measured radiation value is lower than the threshold  $E$ , the direction of movement will change again, from vector  $e_2$  to vector  $e_1$ . Set the movement step size of the UGV as  $s$ . Then, the next measurement position  $x_{i+1}$  can be calculated by

$$x_{i+1} = x_i + s e_{k_1} \quad (3)$$

where  $e_{k_1}$  represents the direction of movement of the UGV, which can be determined by

$$e_i = \begin{cases} e_1, & \text{if Maximum radiation measurement value} < \text{threshold} \\ e_2, & \text{otherwise} \end{cases} \quad (4)$$

After each radiation measurement, the radiation field distribution map will be updated, and then the next measurement position will be predicted. In addition, the next measurement position is only related to the current measurement, that is, the previous measurements will not affect the selection of the next measurement position. The radiation measurement task ends until the exploration path forms a closed loop. Let the set of line segments formed by two consecutive points in the  $n$  radiation measurement point set be  $D_1 = \{a_i\}_{i=1}^{n-1}$ . If  $a_{n-1}$  and  $a_i$  ( $1 \leq i \leq n-2, i \in \mathbb{Z}$ ) satisfy that the condition  $a_{n-1} \cap a_i = 1$ , the UGV continues to perform the radiation measurement task. Otherwise, the execution of the path planning algorithm is terminated. The path

planning algorithm is designed as follows:

**Algorithm 1.** Path planning algorithm

---

```

1: Input: the  $i$  th measurement position  $x_i$  and its corresponding radiation value  $y_i$ 
2: Initialize RID FLAG to 1, switch threshold  $E$ , determine step size  $s$ 
3: while “ $a_{n-1} \cap \forall i = 1, i \in [1, n-2]$ ” do
4:   if RID FLAG then
5:     Select the direction with the highest probability of moving according to Eq.(10)
6:     Calculate the next measurement position  $x_{i+1}$ 
7:     if  $y_i \geq E$  then
8:       Set RID FLAG to 0
9:     end if
10:   else
11:     if  $y_i < E$  then
12:       Select the vector  $e_1$ 
13:     else
14:       Select the vector  $e_2$ 
15:     end if
16:     Calculate the next measurement position  $x_{i+1}$ 
17:   end if
18: end while
19: Output: the next measurement position  $x_{i+1}$ 
```

---

### 2.2.2. The radiation field reconstruction model based on Gaussian Process regression

After the UGV collects the discrete radiation data in the radiation area through the radiation sensor, the two-dimensional (2D) radiation field of detection plane needs to be reconstructed. Several studies have been carried out to reconstruct the radiation field of radioactive sources [17–20]. In this study, the Gaussian process regression (GPR) model is employed to reconstruct the radiation field around the radioactive source. The GPR model is a machine learning algorithm based on Bayesian network, which has good adaptability for dealing with small sample, nonlinear and high-dimensional problems [28,29]. Since the intensity of the radiation dose is related to the distance from the source, the radiation field around the source can be reconstructed by using the radiation measurement points around the source. As a probability prediction method, the GPR model can realize the regression analysis of radiation fields by combining uncertainty estimation with hyperparameter characterization and model training. The GPR model is derived as follows.

For a data set  $D = \{(x_i, y_i)\}_i^n$ ,  $x_i$  and  $y_i$  represent input and output data matrices, respectively. Then, in a finite set of data set  $D$ ,  $f(x^1), f(x^2), \dots, f(x^n)$  can constitute a set of random variables and have a joint Gaussian distribution. Thus, a Gaussian Process (GP) can be defined as follows:

$$f(x) \sim GP(m(x), k(x, x')) \quad (5)$$

where  $m(x)$  is the mean function of the GP;  $k(x, x')$  is the covariance function of the GP. In order to solve the regression problem, the following model can usually be established:

$$y = f(x) + \epsilon \quad (6)$$

where  $x$  is the input vector;  $f(x)$  is the function value;  $y$  is the observation value polluted by additive noise;  $\epsilon$  is the independent Gaussian white noise that obeys the distribution of  $N(0, \delta_n^2)$ , where  $\delta_n$  represents the standard deviation of the noise. The prior distribution of the observed value  $y$  can be obtained as:

$$y \sim N(0, K(X, X) + \delta_n^2 I_n) \quad (7)$$

where  $K(X, X)$  is a symmetric positive definite covariance matrix of order  $n \times n$ , and the element  $k_{ij}$  in matrix  $K(X, X)$  is used to measure the correlation between  $x_i$  and  $x_j$ ;  $I_n$  is an  $n$ -dimensional identity matrix. Further, the joint prior distribution of the observed value  $y$  and the predicted value  $f_*$  can be derived:

$$\begin{bmatrix} y \\ f_* \end{bmatrix} \sim N\left(0, \begin{bmatrix} K(X, X) + \delta_n^2 I_n & K(X, x_*) \\ K(x_*, X) & K(x_*, x_*) \end{bmatrix}\right) \quad (8)$$

where  $K(X, x_*)$  is the  $n \times 1$  order covariance matrix between the test point  $x_*$  and the input  $X$  of the training set, and  $K(X, x_*) = K(x_*, X)^T$ ;  $K(x_*, x_*)$  is the covariance of the test point  $x_*$  itself. Therefore, the posterior probability distribution of the predicted value  $f_*$  can be calculated as:

$$f_* | X, y, x_* \sim N(m_*, Cov(f_*)) \quad (9)$$

where  $m_*$ ,  $Cov(f_*)$  are the mean and variance of the predicted value  $f_*$  corresponding to  $x_*$ , respectively.  $m_*$  can be obtained by the following formula:

$$m_* = K(x_*, X) [K(X, X) + \delta_n^2 I_n]^{-1} y \quad (10)$$

$Cov(f_*)$  can be obtained by the following formula:

$$Cov(f_*) = K(x_*, x_*) - K(x_*, X) [K(X, X) + \delta_n^2 I_n]^{-1} K(X, x_*) \quad (11)$$

In addition, when training a GPR model, it is necessary to choose an appropriate covariance function (or kernel function). The square exponential covariance function is a commonly used covariance function, which can be effectively applied to multivariate nonlinear fitting. Square exponential covariance function is represented by

$$k(x, x') = \sigma_f^2 e^{-\frac{1}{2}(x-x')^T M^{-1} (x-x')} \quad (12)$$

where  $M = \text{diag}(l^2)$ .  $\sigma_f$  and  $l$  are the hyperparameters of the covariance function, and are used to express the characteristics of the width and length scale, respectively. The hyperparameters  $\sigma_f$  and  $l$  can be optimized by the maximum likelihood estimation (MLE) method:

$$\log p(y | \sigma_f, l) = -\frac{1}{2} y^T K_y^{-1} y - \frac{1}{2} \log |K_y| - \frac{n}{2} \log (2\pi) \quad (13)$$

where  $K_y = K(X, X) + \delta_n^2 I_n$ . When training the GPR model, the coordinates of radiation measuring points are used as the input of the model, and the radiation values are used as the output of the model. Then, the trained regression model is used to predict the radiation value of each grid in the occupancy grid map to reconstruct the radiation field distribution of radioactive sources. The radiation field reconstruction algorithm is as follows:

**Algorithm 2.** Radiation field reconstruction algorithm.

---

```

1: Input: the coordinates of the radiation measuring points  $x_i$  and their corresponding
radiation values  $y_i$  ( $1 \leq i \leq n, k \in Z$ )
2: Initialize the hyperparameters  $\sigma_f$  and  $l$  of the covariance function  $k(x, x')$ 
3: Initialize the mean function  $m(x)$  and divide the radiation area into  $m \times n$  grids
4: Solve the optimal combination of  $\sigma_f$  and  $l$  according to Eq.(9)
5: Derive the covariance function  $k(x, x')$  according to Eq.(8)
6: Calculate the mean  $m_*$  and covariance  $Cov(f_*)$  of the input data respectively
according to Eq.(6) and Eq.(7)
7: Derive the joint prior distribution of the observed value  $y$  and the predicted value  $f_*$ 
according to Eq.(4)
8: while “radiation value prediction in  $m \times n$  grids not done” do
9:   Calculate the predicted value  $f_*$  in the remaining grids according to Eq.(5)
10: end while
11: Output: reconstructed radiation field in the occupancy grid map
```

---

### 2.2.3. Estimation of source location based on peak analysis method

After the radiation field has been reconstructed, an important goal is to determine the location of unknown radioactive sources in the area based on the reconstruction result. In homogeneous air [30], the exposure dose rate  $X$  at the distance  $R$  from the point radioactive source can be calculated by

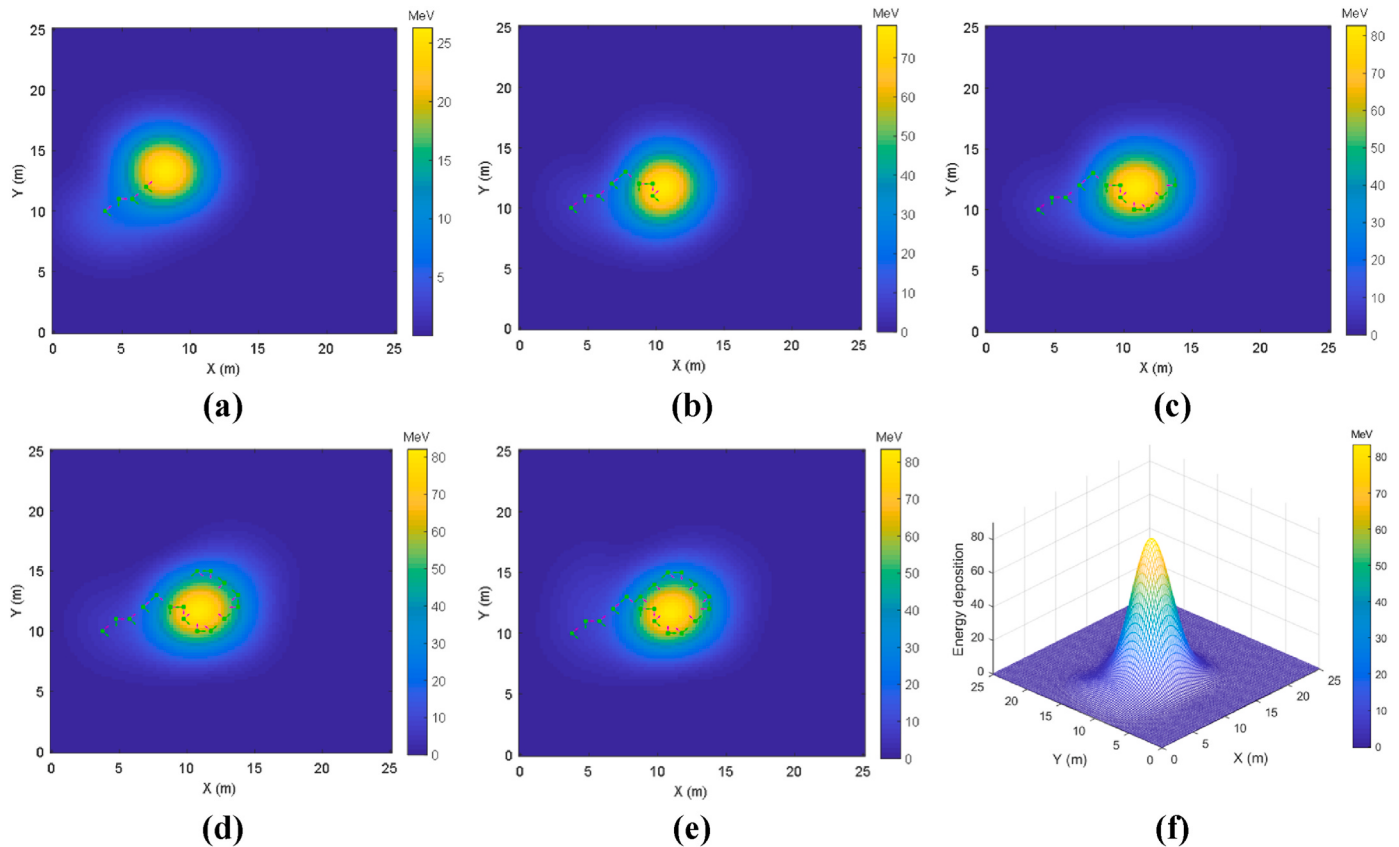


**Fig. 4.** The planned exploration path and radiation field reconstruction results. The small green squares represent the radiation measurement points, and the magenta arrow and the green arrow represent the moving direction vectors  $e_1$  and  $e_2$ , respectively. (a)  $k_2 = 4$ , (b)  $k_2 = 8$ , (c)  $k_2 = 12$ , (d)  $k_2 = 16$  and (e)  $k_2 = 18$ . (f) Reconstructed radiation field at the number of measurements  $k_2 = 18$ , where the Z axis (Energy deposition) represents the radiation value. (For interpretation of the references to color in this figure legend, the reader is referred to the Web version of this article.)

$$X = \Gamma \frac{A}{R^2} \quad (14)$$

where  $\Gamma$  is the exposure dose rate constant;  $A$  is the activity of the point radioactive source;  $R^2 = (x - x_0)^2 + (y - y_0)^2$ , and  $(x_0, y_0)$  is the coordinate of the source. Therefore, when  $x \rightarrow x_0$  and  $y \rightarrow y_0$ , the exposure dose rate  $X$  will get a peak. In other words, for a single radioactive source, the coordinate corresponding to the peak of exposure dose rate in the radiation field is the location of the source.

When there are  $n$  point radioactive sources in the area, the location coordinates of the sources are respectively  $(x_1, y_1), (x_2, y_2), \dots, (x_n, y_n)$ , and the corresponding activities of each source are respectively  $A_1, A_2, \dots, A_n$ . Similarly, the exposure dose rate  $X$  at  $(x, y)$  can be calculated by

$$X = \sum_i^n \Gamma \frac{A_i}{(x - x_i)^2 + (y - y_i)^2} \quad (15)$$

According to formula (15), the radiation field formed by multiple point radioactive sources will have peaks at  $(x_1, y_1), (x_2, y_2), \dots, (x_n, y_n)$ . Therefore, by analyzing the number of peaks and their corresponding coordinates in the reconstructed radiation field, the number and location of radioactive sources in the area can be determined. This method of source location estimation is known as peak analysis.

### 3. Results and discussion

In order to verify the feasibility and effectiveness of the proposed method for source localization, simulation verification experiments were carried out in the scenarios with single and two gamma radioactive sources respectively in Section 3.1. In particular, we further analyzed

the cases where the two sources have the same or different activity of the same order of magnitude, and the cases where the two sources are separated or close to each other. In addition, we discussed the impact of different threshold settings on the UGV's exploration path and reconstruction results. In Section 3.2, an UGV equipped with radiation detectors was used to carry out the real source localization experiment on a Cs-137 point source.

#### 3.1. Simulation experiment and analysis

##### 3.1.1. Autonomous localization of single radioactive source

In the simulation environment, the type of radioactive source is set to gamma source. In the case of single source, the source with an activity of 2 mCi and an energy of 1.33 MeV is placed at (11.0 m, 12.0 m). Then, the energy deposition of gamma rays in space is approximated using the Geant4 program based on the MC method. Furthermore, the threshold is set as  $E = 50$  and the step size is set as  $s = 1$  m. In the process of source search, the next measurement position of the UGV will be automatically predicted by Algorithm 1, and then the reconstructed radiation field is updated after each radiation measurement by Algorithm 2.

When the initial position of the UGV is (10.0 m, 3.75 m), the planned exploration path and final reconstructed radiation field are shown in Fig. 4(e). Fig. 4(a)–(e) show the radiation field reconstruction results when the number of measurements is  $k_2 = 4, k_2 = 8, k_2 = 12, k_2 = 16$ , and  $k_2 = 18$ , respectively. Since the radiation measurements from first to seventh are less than the threshold  $E$ , the UGV moves in the direction of the vector  $e_1$  to approach the radioactive source. After completing the 8th measurement, due to the measurement value exceeding the threshold  $E$ , the exploration direction of the UGV begins to change from  $e_1$  to  $e_2$  to move around the source. In particular, since the radiation

**Table 1**

Source location estimation error for different number of radiation measurements.

The number of measurement	Estimated source location (m)	Source location estimation error (m)
4	(8.08, 13.13)	(2.92, 1.13)
8	(10.35, 11.62)	(0.65, 0.38)
12	(10.61, 11.87)	(0.39, 0.13)
16	(10.86, 11.62)	(0.14, 0.38)
18	(10.86, 11.62)	(0.14, 0.38)

measurements from the 8th to 18th exceed the threshold  $E$ , the direction of movement has been maintained to  $e_2$  during this period. When the UGV continues to move to the predicted next position, the path planning algorithm terminates the execution due to the closed loop formed by the exploration path. Fig. 4(f) shows the reconstructed radiation field at the number of measurements  $k_2 = 18$ . According to formula (14), the coordinate corresponding to the peak of energy deposition in the reconstructed radiation field is considered to be the estimated location of the radioactive source. Table 1 shows the source estimation location and error from true source location at the number of measurements  $k_2 = 4$ ,  $k_2 = 8$ ,  $k_2 = 12$ ,  $k_2 = 16$  and  $k_2 = 18$ , respectively. It can be seen from Table 1 that as the number of measurements increases, the source

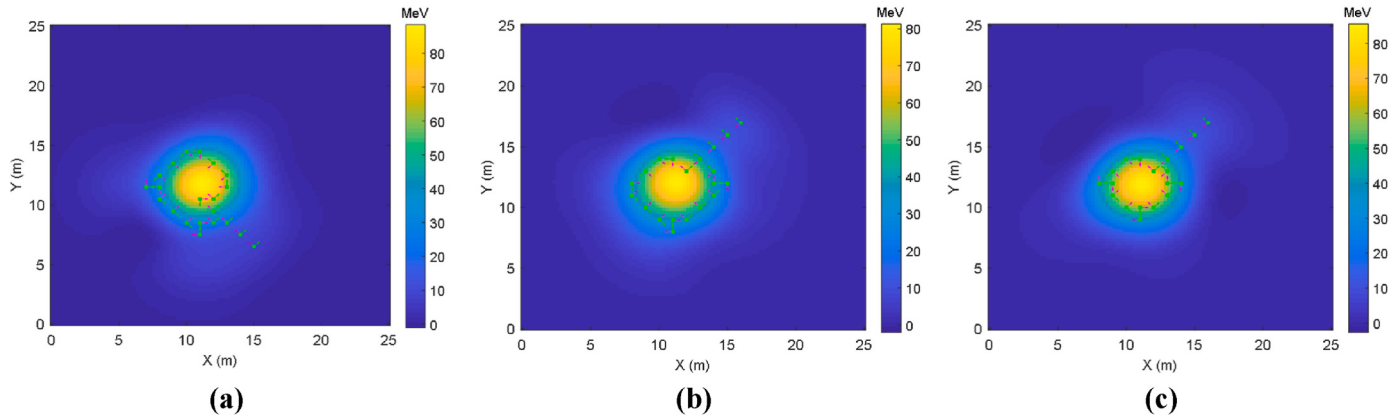


**Fig. 5.** The impact of different initial positions and thresholds  $E$  on the planned exploration path and radiation field reconstruction result. (a) The initial position is (15.0 m, 6.5 m) and the threshold is set as  $E = 50$ . (b) The initial position is (16.0 m, 17.0 m) and the threshold is set as  $E = 50$ . (c) The initial position is (16.0 m, 17.0 m) and the threshold is set as  $E = 80$ .

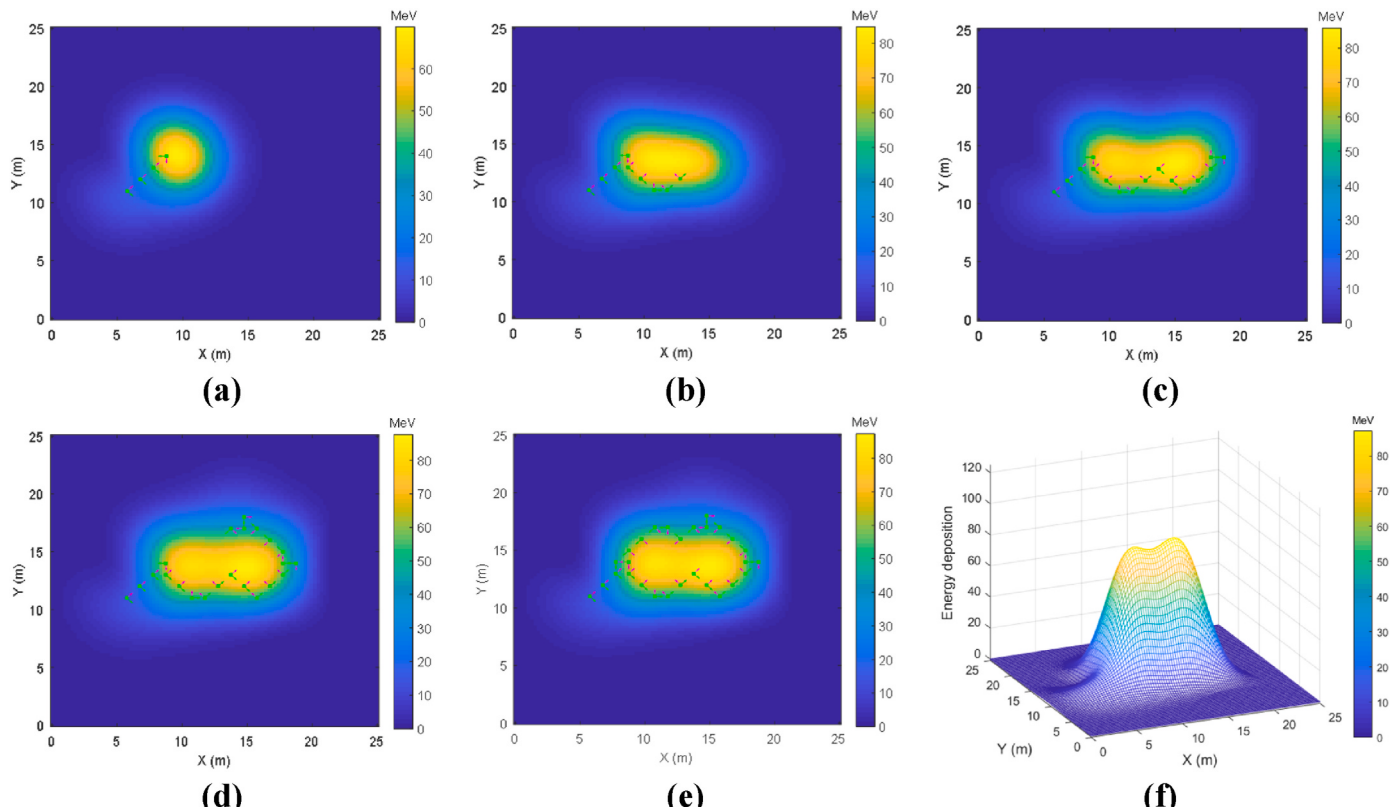


**Fig. 6.** The planned exploration path and radiation field reconstruction result for the locations of two sources that are dispersed. (a)  $k_2 = 4$ , (b)  $k_2 = 9$ , (c)  $k_2 = 16$ , (d)  $k_2 = 22$  and (e)  $k_2 = 28$ . (f) Reconstructed radiation field at the number of measurements  $k_2 = 28$ .

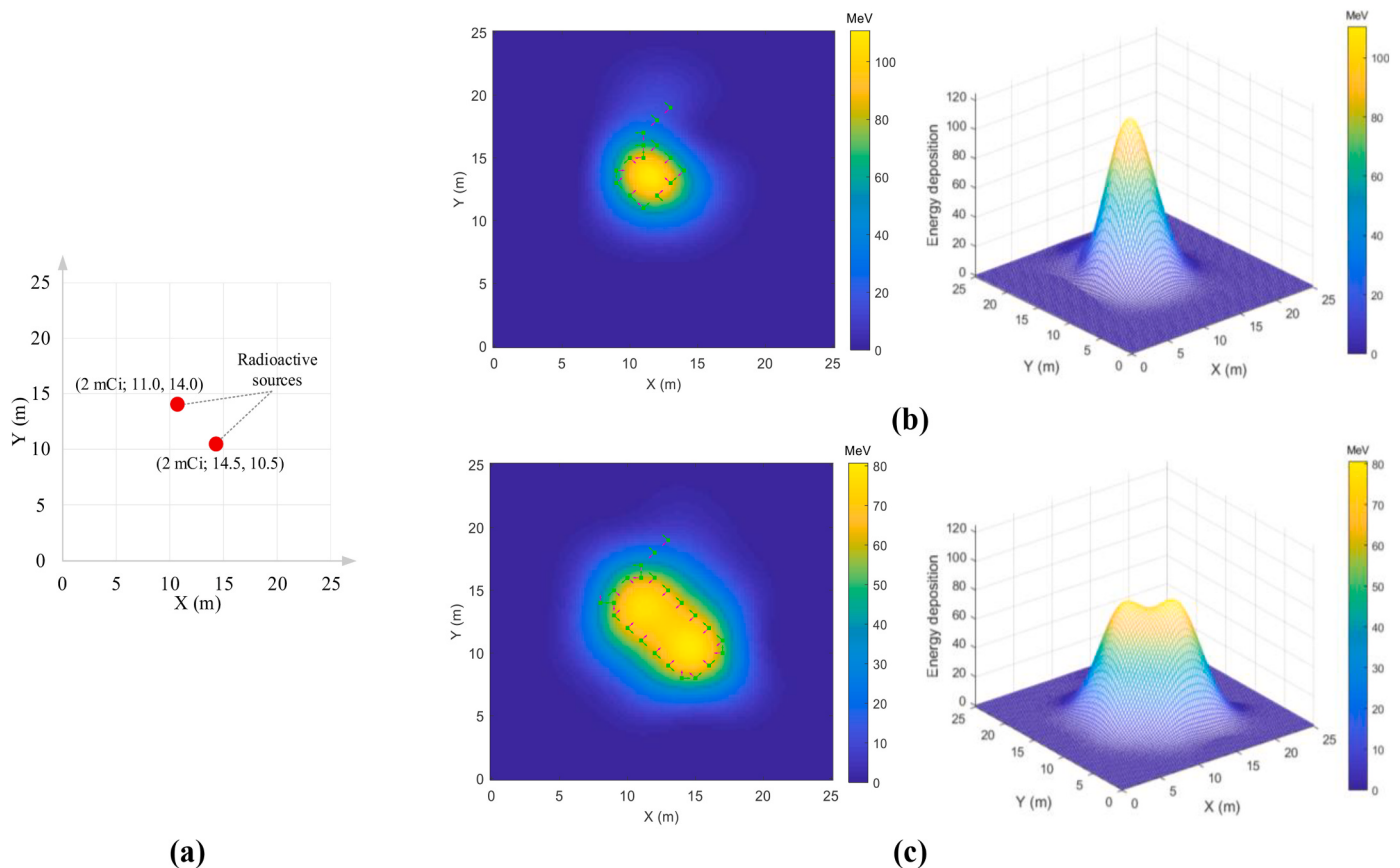


**Fig. 7.** The impact of different thresholds on the exploration path and the final reconstruction result. (a) Schematic diagram of the location distribution of two sources. (b)  $E = 90$ . (c)  $E = 60$ .

location estimation error of the PRE method is gradually decreasing. When the number of measurements  $k_2 = 18$ , the error between the estimated source location and the true source location is reduced to approximately 0.40 m.

Plot (a) and (b) of Fig. 5 respectively show the exploration paths and radiation field reconstruction results obtained at different initial positions when the threshold is set as  $E = 50$ . When the initial position of the UGV is (15.0 m, 6.5 m), the path planning task is completed after 21 radiation measurements, and then the radiation field of the radioactive source is reconstructed. Similarly, the reconstructed radiation field have a peak, and the coordinate corresponding to the peak represents the estimated source location. The error between the estimated source location and the actual source location is approximately 0.40 m. When the initial position of the UGV is (16.0 m, 17.0 m), the path planning task is completed after 19 radiation measurements. Finally, the radiation field around radioactive source is reconstructed, and the error between the estimated source location and the true source location is approximately 0.38 m. Therefore, the selection of the initial position has little effect on reducing the source location estimation error. Next, we discuss the impact of different threshold settings on path planning and radiation field reconstruction. The threshold is adjusted to  $E = 80$ , and the initial position remains unchanged. Subsequently, the planned exploration path and the reconstructed radiation field are shown in Fig. 5(c), and the error between the estimated source location and the actual source location is approximately 0.38 m. Comparing plot (b) and (c) of Fig. 5, it can be seen that different threshold  $E$  will affect the selection of radiation measure points, resulting in a difference in the reconstructed radiation field.

### 3.1.2. Autonomous localization of two radioactive sources

**3.1.2.1. The case of two radioactive sources with same activity.** In Section 3.1.1, the experimental results demonstrate the feasibility of the PRE method for autonomous localization of single radioactive source. However, there may be more than one radioactive source in the search area, and autonomous localization of multiple radioactive sources is challenging for UGVs. Assuming that there are two gamma sources with the same activity (2 mCi) in the environment, there are two situations for the location of two sources: dispersed or relatively concentrated. Next, we discuss the two situations of source location dispersion and concentration in turn. Initially, the two sources are placed at (10.5 m, 14 m) and (15.5 m, 14 m) respectively. Similarly, the energy deposition of gamma rays emitted by the two sources in space is approximated using the Geant4 program based on Monte Carlo method. Then, the threshold is adjusted to  $E = 60$ .

When the initial position of the UGV is (5.75 m, 11 m), the planned exploration path and final reconstructed radiation field are shown in Fig. 6(e). Fig. 6(a)–(e) show the radiation field reconstruction results when the number of measurements is  $k_2 = 4$ ,  $k_2 = 9$ ,  $k_2 = 16$ ,  $k_2 = 22$ , and  $k_2 = 28$ , respectively. Since the radiation measurements from 1st to 4th are less than the threshold  $E$ , the UGV moved in the direction of the vector  $e_1$  to approach the sources, as shown in Fig. 6(a). At this time, the reconstructed radiation field fails to reflect the location of all sources in the area. After completing the 5th measurement, due to the measurement value exceeding the threshold  $E$ , the exploration direction of the UGV begins to change from  $e_1$  to  $e_2$  to move around the sources. It is not until the 16th measurement that the exploration direction is changed from  $e_2$  to  $e_1$  as the measurement value of the current position is less than the threshold. Similarly, the exploration direction after the 21st measurement is also changed from  $e_2$  to  $e_1$ . However, since the radiation

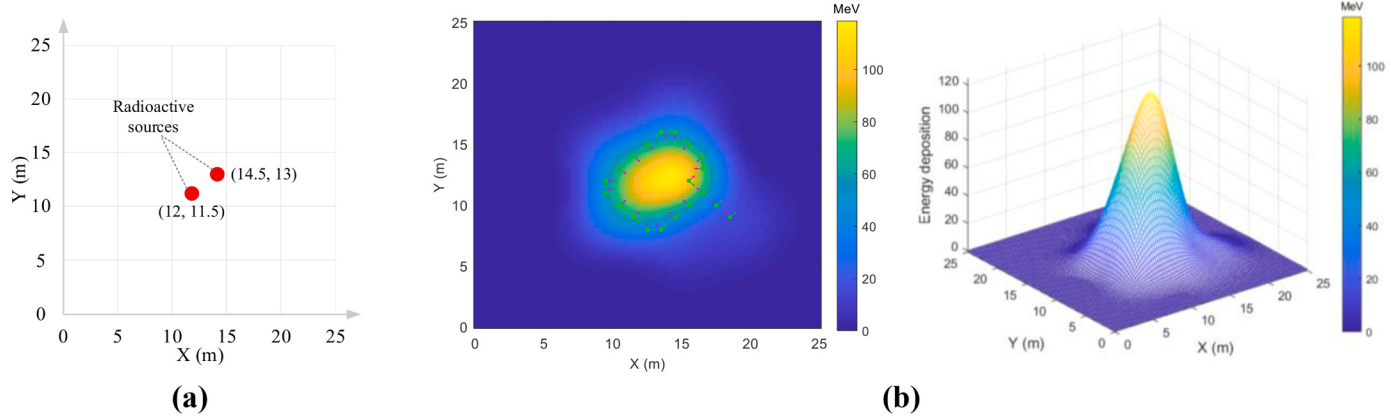


**Fig. 8.** The planned exploration path and reconstructed radiation field for the locations of two sources that are concentrated. (a) Schematic diagram of the location distribution of two radioactive sources. (b) Reconstructed radiation field at the number of measurements  $k_2 = 20$ .

measurements from the 17th to the 20th and from the 22nd to the 28th exceed the threshold, the UGV always moved in the direction of the vector  $e_2$ . Fig. 6(f) shows the reconstructed radiation field at the number of measurements  $k_2 = 28$ . By the peak analysis method, the respective coordinates (10.86 m, 13.89 m) and (15.15 m, 13.64 m) corresponding to two obvious peaks in the reconstructed radiation field is considered to be the estimated source locations. Therefore, the errors between the two estimated source locations and the two true source locations are approximately 0.38 m and 0.50 m, respectively.

To discuss the impact of different threshold settings on path planning and radiation field reconstruction, the thresholds are set to  $E = 90$  and  $E = 60$ , respectively. Fig. 7(a) shows the location distribution of two radioactive sources. The true locations of two sources are (11.0 m, 14.0 m) and (14.5 m, 10.5 m) respectively, and the initial position of the UGV is (13.0 m, 19.0 m). Plot (b) and (c) of Fig. 7 show the planned exploration paths and radiation field reconstruction results when the threshold are  $E = 90$  and  $E = 60$ , respectively. When the threshold is  $E = 60$ , the locations of two sources can be estimated by the reconstructed radiation field based on the peak analysis method, and the error from the true source location is 0.51 m and 0.19 m, respectively. However, when the threshold is selected as  $E = 90$ , the planned exploration path only surrounds one of the two sources, resulting in the inability to estimate the locations of all sources through the reconstructed radiation field. Therefore, choosing an appropriate threshold is of vital important to locate all radioactive sources in the area.

Next, we analyze the situation that the locations of two radioactive sources are relatively concentrated. Fig. 8(a) shows the location

distribution of two radioactive sources. The true locations of two sources are (12.0 m, 11.5 m) and (14.5 m, 13.0 m), respectively. Then, the threshold is set as  $E = 60$ , and the initial position of the UGV is (18.5 m, 9.0 m). Fig. 8(b) shows the planned exploration path and reconstructed radiation field. Due to the effect of source location concentration, the peak analysis method which only estimates one location through the reconstructed radiation field fails to determine the respective locations of two sources in the area. However, the error between the estimated source location (14.14 m, 12.37 m) and the central location (13.75 m, 12.25 m) of two true radioactive sources is only 0.41 m, indicating that the PRE method can effectively plan the exploration path and reconstruct the radiation field in the scenario of two radioactive sources with same activity that are close to each other.

**3.1.2.2. The case of two radioactive sources with different activity.** Considering that there are two gamma sources with the different activity of the same order of magnitude (the activity of one source is 1 mCi, and the activity of the other source is 2 mCi) in the environment. Similarly, there are two situations for the locations of two sources, i.e. dispersed or relatively concentrated. First, we discuss the situation of source location dispersion. As shown in Fig. 9(a), two sources are placed at (12.5 m, 9.0 m) and (12.5 m, 14.0 m) respectively. The energy deposition of gamma rays emitted by the two sources in space is approximated by the Geant4 program. The threshold is adjusted to  $E = 50$ , and the initial position of the UGV is (10.5 m, 18.0 m). Subsequently, the next measurement position of the UGV will be automatically predicted by Algorithm 1, and then the reconstructed radiation field is updated after each radiation

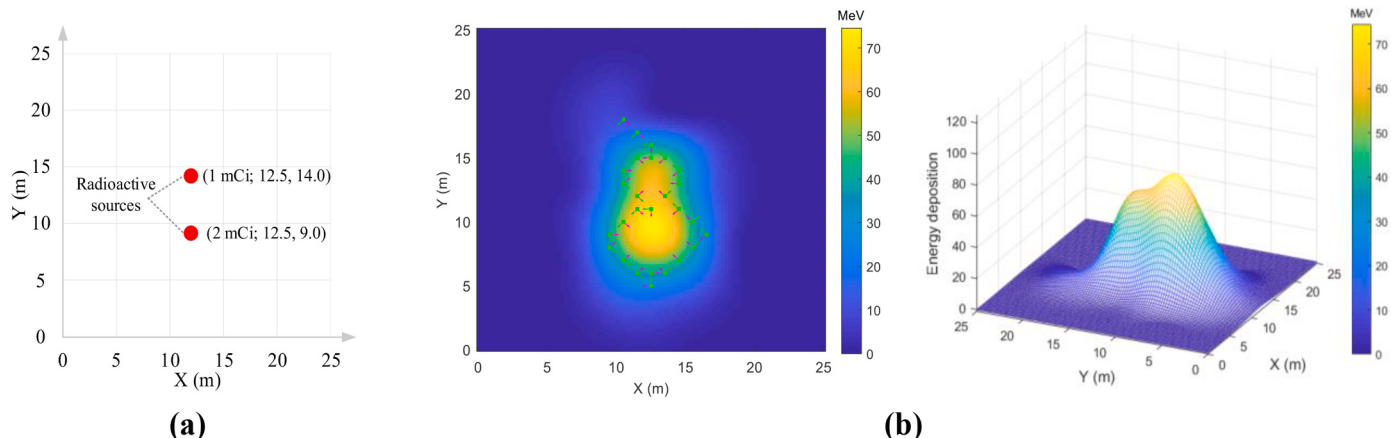


**Fig. 9.** The planned exploration path and reconstructed radiation field for the locations of two sources that are dispersed. (a) Schematic diagram of the location distribution of two radioactive sources. (b) Reconstructed radiation field at the number of measurements  $k_2 = 27$ .

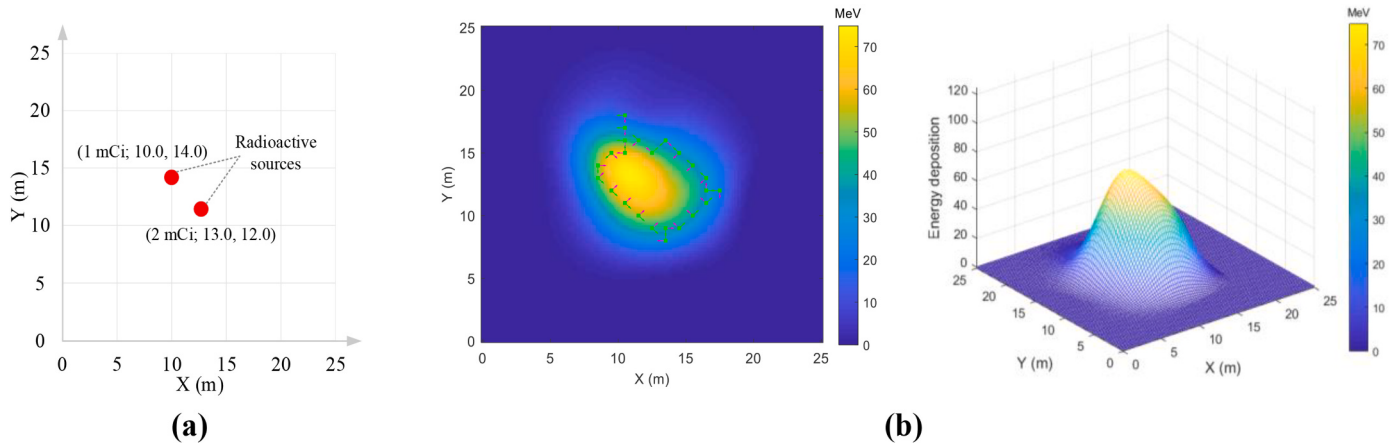


**Fig. 10.** The planned exploration path and reconstructed radiation field for the locations of two sources that are concentrated. (a) Schematic diagram of the location distribution of two radioactive sources. (b) Reconstructed radiation field at the number of measurements  $k_2 = 24$ .

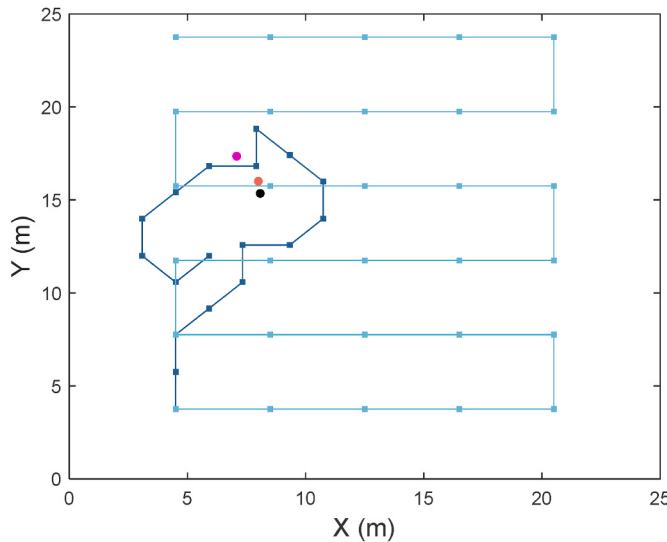


**Fig. 11.** Comparative experiments on source localization between the uniform deterministic search method and the proposed method. The orange dot represents the true source location; the black dot represents the estimated source location of the proposed method; the pink dot represents the estimated source location of the uniform deterministic search method. (For interpretation of the references to color in this figure legend, the reader is referred to the Web version of this article.)

measurement by Algorithm 2. Fig. 9(b) shows the planned exploration path, and the reconstructed radiation field at the number of measurements  $k_2 = 27$ . It can be seen from Fig. 9(b) that although the two sources have different activities, the PRE method can still plan an effective exploration path and reconstruct the radiation field around the radioactive source. Based on the reconstructed radiation field, it can be estimated using the peak analysis method that there are two radioactive sources in the area, and their locations are (12.63 m, 9.59 m) and (12.63 m, 13.89 m), respectively. Therefore, the errors between the two estimated source locations and the two true source locations are approximately 0.60 m and 0.17 m, respectively.

The locations of the two sources may also be relatively concentrated, as shown in Fig. 10(a). In Fig. 10(a), the two sources are located at (13.0 m, 12.0 m) and (10.0 m, 14.0 m) respectively. The threshold  $E$  and initial position of the UGV are unchanged. Fig. 10(b) shows the planned exploration path, and the reconstructed radiation field at the number of measurements  $k_2 = 24$ . Since two sources are close to each other, the

**Table 2**  
Performance comparision of the proposed method with previous methods.

	Uniform deterministic	Random walk	Proposed
The number of measurement	30	18	18
Source location estimation error in X (m)	1.07	3.17	0.08
Source location estimation error in Y (m)	1.35	2.83	0.55

peak analysis method only estimates one location through the reconstructed radiation field and fails to determine the respective locations of two sources in the area. However, the error between the estimated source location (11.06 m, 13.38 m) and the central location of the two true sources is only 0.58 m, indicating that the PRE method can also effectively plan the exploration path and reconstruct the radiation field in the scenario of two radioactive sources with the different activity of the same order of magnitude that are close to each other.

### 3.1.3. Performance comparision

In order to verify the effectiveness of the proposed method, comparative experiments are carried out with the existing uniform deterministic search method and random walk method [31,32]. In the simulation environment, one source with an activity of 4 mCi is placed in a 25 m × 25 m rectangular search area, and the true location of the source is (8.0 m, 16.0 m). The distance between radiation measurement points is assumed to be 2 m, and the threshold is set to 45. Fig. 11 shows the comparative experiments on source localization between the uniform deterministic search method and the proposed method (random walk not shown). In the comparative experiment, the GPR model is used to reconstruct the radiation field and the source location is determined from the reconstructed radiation field. The orange dot represents the true source location; the black dot represents the estimated source location of the proposed method; the pink dot represents the estimated source location of the uniform deterministic search method. For the random walk method, we take the average error of twenty experimental results as the source location estimation error. Table 2 shows the performance comparision of the proposed method with the uniform deterministic search and random walk method. It can be seen from Table 2 that the proposed method can achieve higher source localization accuracy with fewer radiation measurements than two previous method, which demonstrates the effectiveness and superiority of the proposed method. Compared with the random walk, the source localization accuracy of the proposed method is increased by approximately 86.91 %.

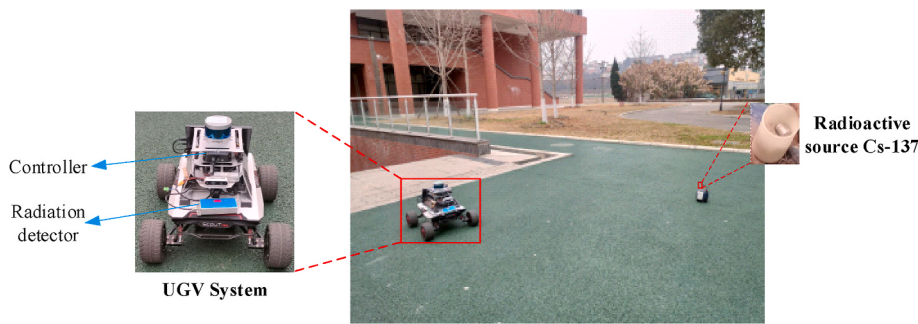


Fig. 12. Radioactive source localization experiment in a real-world scenario.

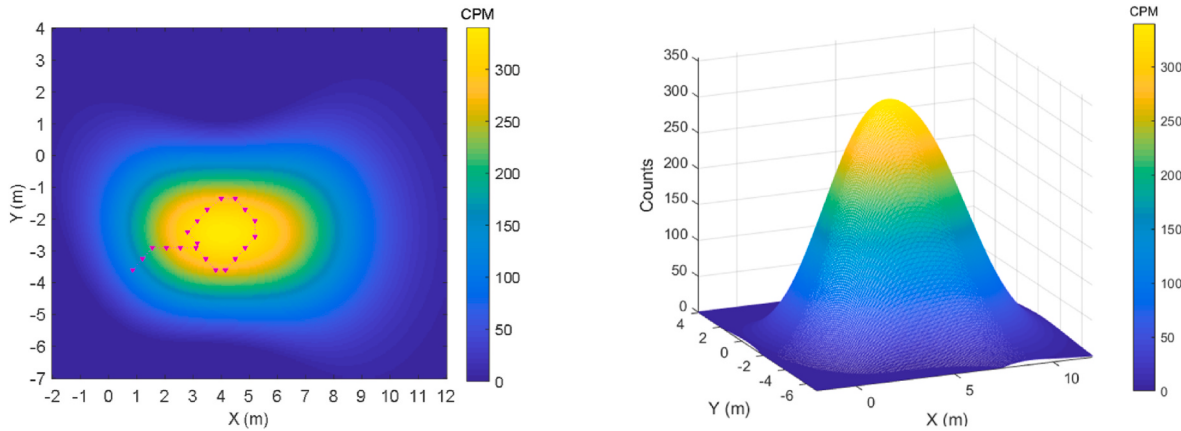


Fig. 13. The planned exploration path of the UGV and radiation field reconstruction results. The small magenta triangles indicate radiation measurement points.

### 3.2. Real experiment and analysis

To further verify the feasibility of the PRE method, an UGV equipped with a radiation detector similar to the Geiger-Müller counter is used to carry out the autonomous localization experiment for single radioactive source Cs-137 in a real-world scenario (the PRE method can be applicable to different types of ray sources, and the setting of search threshold needs to refer to the source parameter information). The radiation detector is mounted at a horizontal distance of approximately 0.2 m from the central axis of the UGV, which can collect radiation data in eight directions around the current position by rotating the UGV. Limited by the type of the radiation detector equipped on the UGV, the detector can only calculate the radiation dose or counts (radiation dose or counts and energy deposition can be converted to each other [32]). The activity of the radioactive source Cs-137 is approximately 1 mCi, and the average energy of gamma rays emitted by the radioactive source is approximately 0.662 MeV. Fig. 12 shows the physical image of the UGV system as well as the image of the real experimental scenario. In this scenario, the Cs-137 point source is located at (4.53 m, -2.48 m), and the natural background counts measured by the detector at infinity from the radioactive source is 24 CPM (CPM indicates the number of photons recorded per minute). To better reconstruct the radiation field, the natural background counts will be deducted from each measurements.

Due to the limited sensing ability of the detector, the count value of each direction around the UGV's current position  $x_i$  within the same duration  $\Delta t$  is measured separately to calculate the radiation gradient. Then, the radiation value  $y_i$  at the current position is represented by the measured value in the direction of the maximum radiation gradient. In addition, the odometer which is integrated into the UGV system can obtain the UGV's current coordinates, and the equipped controller can execute Algorithm 1 to predict the next measurement position. The measurement positions and their corresponding radiation

Table 3

Source location estimation error for different number of radiation measurements.

The number of measurement	Estimated source location (m)	Source location estimation error (m)
4	(2.67, -2.48)	(1.86, 0.28)
8	(3.37, -2.43)	(1.16, 0.33)
12	(4.02, -2.03)	(0.51, 0.73)
16	(4.76, -2.58)	(0.23, 0.18)
20	(4.27, -2.63)	(0.26, 0.13)

measurements will be wirelessly transmitted to an Industrial Control Computer to carry out the radiation field reconstruction and source location estimation.

In this experiment, the UGV moves in fixed steps of 0.5 m, and the initial position of the UGV is (0.85 m, -3.6 m). Taking into account the effect of source activity, the threshold  $E$  is set as 300 (CPM). The next measurement position of the UGV is predicted by the path planning algorithm (Algorithm 1), and the radiation field distribution around the radioactive source will be reconstructed by the radiation field reconstruction algorithm (Algorithm 2). Fig. 13 shows the planned exploration path and reconstructed radiation field. Table 3 shows the estimated source locations and their corresponding errors from true source location under different number of radiation measurements. It can be seen from Table 3 that as the increase of the number of measurements, the error between the estimated source location and the true source location is gradually decreasing. When the UGV completes the radiation measurement task at the number of measurements  $k_2 = 20$ , the error of source location estimation has been reduced to approximately 0.30 m. Therefore, the experimental result demonstrated that the PRE method had good performance in source localization accuracy.

#### 4. Conclusion

In this study, a source localization method suitable for UGVs that can only obtain sparse measurements within limited exploration time is proposed to locate radioactive sources through path planning, radiation field reconstruction and source location estimation. The designed path planning algorithm can actively predict the next measurement position of the UGV to plan the exploration path and obtain effective radiation data, and the radiation field reconstruction algorithm based on GPR model can utilize sparse radiation data to reconstruct the radiation field around radioactive sources. Then, the locations of radioactive sources can be determined through the reconstructed radiation field. Extensive simulation experiments show the feasibility and effectiveness of the proposed method. In a real experimental scenario, the proposed method can make the UGV autonomously explore and locate the radioactive source Cs-137 with the localization accuracy of approximately 0.30 m. In addition, it is worth noting that the proposed method is also suitable for autonomous localization in scenarios with two sources which are different or same activity by setting appropriate threshold.

However, when the activities of sources differ by orders of magnitude or the locations of multiple radioactive sources are relatively concentrated, the proposed method may fail to determine the respective locations of all sources. In the future, we would like to solve this problem by using appropriate methods such as contour similarity analysis [33, 34] and introduce radiation array sensors. Moreover, obstacles in the environment can shield or interfere with gamma rays, affecting the planned exploration path and source location estimation, and the experiments in more complex scenarios such as terrain restrictions and obstacle occlusion will be conducted to further improve the proposed method.

#### Author contributions

Conceptualization, J.W. and Y.Z.; methodology, investigation and writing—original draft preparation X.H.; software, J.H. and X.H.; validation, Y.G., J.W. and X.H.; resources, J.W. and Y.Z.; writing—review and editing, J.H. and Y.Z.; visualization, Y.G.; supervision and project administration, L.H.; funding acquisition, J.W. and J.H. All authors have read and agreed to the published version of the manuscript.

#### Declaration of interest statement

The authors declare that they have no known competing financial interests or personal relationships that could have appeared to influence the work reported in this paper.

#### Acknowledgments

This research was funded by the National Natural Science Foundation of China (No.12205245), Natural Science Foundation of Sichuan Province (No.2023NSFSC1437), NHC Key Laboratory of Nuclear Technology Medical Transformation (Mianyang Central Hospital) (No. 2021HYX16), and State Administration of Science , Technology and Industry for National Defense (No. JCKY2020404C001).

#### References

- [1] IAEA Incident and Trafficking Database (ITDB). Incidents of Nuclear and Other Radioactive Material Out of Regulatory Control. Available online: <https://www.iaea.org/sites/default/files/22/01/itdb-factsheet.pdf> (accessed on 10 February 2023).
- [2] Y. Zhou, N. Yu, J. Wang, W. Chen, P. Cai, Review of the 5·7 Nanjing 192Ir source radiological accident, *Radiation Medicine and Protection* 3 (4) (2022) 190–195.
- [3] J.W. Howse, L.O. Ticknor, K.R. Muske, Least squares estimation techniques for position tracking of radioactive sources, *Automatica* 37 (11) (2001) 1727–1737.
- [4] Y. Huang, J. Benesty, G.W. Elko, R.M. Mersereati, Real-time passive source localization: a practical linear-correction least-squares approach, *IEEE Trans. Speech Audio Process.* 9 (8) (2001) 943–956.
- [5] N.S.V. Rao, M. Shankar, J.C. Chin, D.K. Yau, S. Srivathsan, S.S. Iyengar, Identification of low-level point radiation sources using a sensor network, in: 2008 International Conference on Information Processing in Sensor Networks (IPSN), IEEE, 2008, pp. 493–504, 2008.
- [6] A.H.W. Liu, *Simulation and Implementation of Distributed Sensor Network for Radiation Detection*, California Institute of Technology, 2010.
- [7] H.E. Baidoo-Williams, Maximum Likelihood Localization of Radiation Sources with Unknown Source Intensity, 2016 arXiv preprint arXiv:1608.00427.
- [8] E. Bai, A. Heifetz, P. Raptis, S. Dasgupta, R. Mudumbai, Maximum likelihood localization of radioactive sources against a highly fluctuating background, *IEEE Trans. Nucl. Sci.* 62 (6) (2015) 3274–3282.
- [9] A. Gunatilaka, B. Ristic, R. Gailis, On localisation of a radiological point source, in: 2007 Information, Decision and Control, IEEE, 2007, pp. 236–241, 2007.
- [10] J. Huo, M. Liu, K.A. Neuspin, H. Liu, M. Guo, Y. Xiao, Autonomous search of radioactive sources through mobile robots, *Sensors* 20 (12) (2020) 3461.
- [11] M.P. De, J. Hoffman, Bayesian source reconstruction of an anomalous Selenium-75 release at a nuclear research institute, *J. Environ. Radioact.* 218 (2020), 106225.
- [12] P. Xu, C. Fu, Z.Y. Tan, X.F. Cai, J. Qin, Robust radioactive sources research method using possibility particle filter, *AIP Adv.* 11 (8) (2021), 085308.
- [13] M. Ling, J. Huo, G.V. Moiseev, L. Hu, Y. Xiao, Multi-robot collaborative radioactive source search based on particle fusion and adaptive step size, *Ann. Nucl. Energy* 173 (2022), 109104.
- [14] M.R. Morelande, B. Ristic, Radiological source detection and localisation using Bayesian techniques, *IEEE Trans. Signal Process.* 57 (11) (2009) 4220–4231.
- [15] M. Morelande, B. Ristic, A. Gunatilaka, Detection and parameter estimation of multiple radioactive sources, in: Proceedings of the 10th International Conference on Information Fusion, Quebec, AB, Canada, 9–12 July 2007, 2007, pp. 1–7.
- [16] N.A. Abd Rahman, K.S.M. Sahari, M.F.A. Jalal, A.A. Rahman, M.I. Abd Adziz, M. Z. Hassan, Mobile robot for radiation mapping in indoor environment, in: IOP Conference Series: Materials Science and Engineering, vol. 785, IOP Publishing, 2020, 012021, 1.
- [17] P. Royo, E. Pastor, M. Macias, R. Cuadrado, C. Barrado, A. Vargas, An unmanned aircraft system to detect a radiological point source using RIMA software architecture, *Rem. Sens.* 10 (11) (2018) 1712.
- [18] B. Li, Y. Zhu, Z. Wang, C. Li, Z.R. Peng, L. Ge, Use of multi-rotor unmanned aerial vehicles for radioactive source search, *Rem. Sens.* 10 (5) (2018) 728.
- [19] X. Liu, L. Cheng, Y. Yang, G. Yan, X. Xu, Z. Zhang, An alpha/beta radiation mapping method using simultaneous localization and mapping for nuclear power plants, *Machines* 10 (9) (2022) 800.
- [20] T. Kishimoto, H. Woo, R. Komatsu, Y. Tamura, H. Tomita, K. Shimazoe, A. Yamashita, H. Asama, Path planning for localization of radiation sources based on principal component analysis, *Appl. Sci.* 11 (10) (2021) 4707.
- [21] S. Li, R. Kong, Y. Guo, Cooperative distributed source seeking by multiple robots: algorithms and experiments, *IEEE/ASME Trans. mech.* 19 (6) (2014) 1810–1820.
- [22] P. Proctor, C. Teuscher, A. Hecht, M. Osiński, Proximal policy optimization for radiation source search, *J. Nucl. Eng.* 2 (4) (2021) 368–397.
- [23] Z. Liu, S. Abbaszadeh, Double Q-learning for radiation source detection, *Sensors* 19 (4) (2019) 960.
- [24] Y. Ji, Y. Zhao, B. Chen, Z. Zhu, Y. Liu, H. Zhu, S. Qiu, Source searching in unknown obstructed environments through source estimation, target determination, and path planning, *Build. Environ.* 221 (2022), 109266.
- [25] H. Tomita, S. Hara, A. Mukai, K. Yamagishi, H. Ebii, K. Shimazoe, Y. Tamura, H. Woo, H. Takahashi, H. Asama, F. Ishida, E. Takada, J. Kawarabayashi, K. Tanabe, K. Kamada, Path-planning system for radioisotope identification devices using  $4\pi$  gamma imaging based on random forest analysis, *Sensors* 22 (12) (2022) 4325.
- [26] H.I. Lin, Search strategy of a mobile robot for radiation sources in an unknown environment, in: 2014 International Conference on Advanced Robotics and Intelligent Systems (ARIS), IEEE, 2014, pp. 56–60, 2014.
- [27] S. Agostinelli, J. Allison, K.A. Amako, J. Apostolakis, H. Araujo, P. Arce, Geant4 Collaboration, GEANT4—a simulation toolkit, *Nucl. Instrum. Methods Phys. Res. Sect. A Accel. Spectrom. Detect. Assoc. Equip.* 506 (3) (2003) 250–303.
- [28] C.K. Williams, C.E. Rasmussen, *Gaussian Process for Machine Learning*, MIT Press, Cambridge, MA, USA, 2006.
- [29] L. Mónes, N. Bernstein, G. Csányi, Exploration, sampling, and reconstruction of free energy surfaces with Gaussian process regression, *J. Chem. Theor. Comput.* 12 (10) (2016) 5100–5110.
- [30] A.J.J. Bos, Fundamentals of radiation dosimetry, *AIP Conf. Proc. Am. Instit. Phys.* 1345 (1) (2011) 5–23.
- [31] B. Ristic, M. Morelande, A. Gunatilaka, Information driven search for point sources of gamma radiation, *Signal Process.* 90 (2010) 1225–1239.
- [32] J. Huo, X. Hu, J. Wang, L. Hu, ACA: automatic search strategy for radioactive source, *Nucl. Eng. Technol.* 55 (2023) 3030–3038.
- [33] J. Towler, B. Krawiec, K. Kochersberger, Radiation mapping in post-disaster environments using an autonomous helicopter, *Rem. Sens.* 4 (7) (2012) 1995–2015.
- [34] A.A.R. Newaz, S. Jeong, H. Lee, H. Ryu, N.Y. Chong, M.T. Mason, Fast radiation mapping and multiple source localization using topographic contour map and incremental density estimation, in: 2016 IEEE International Conference on Robotics and Automation (ICRA), IEEE, 2016, pp. 1515–1521, 2016.